Journal of Non-Crystalline Solids 48 (1982) 47–64
North-Holland Publishing Company



# SOL–GEL TRANSITION IN SIMPLE SILICATES *

C.J. BRINKER, K.D. KEEFER, D.W. SCHAEFER and C.S. ASHLEY

*Sandia National Laboratories **, Albuquerque, New Mexico 87185, USA*

Silicate gels were prepared under a range of conditions in which the rate of hydrolysis was varied from fast to slow with respect to the rate of condensation. When hydrolysis was fast, larger, more highly condensed polymers were formed during gelation. Conversely, for slow hydrolysis, smaller, less highly condensed polymers were formed. These gels dried to low density coarse textured and high density fine textured gels, respectively. High temperatures (>800°C) were required to densify the coarse gels by viscous sintering. Lower temperatures were sufficient to densify fine gels by a process which was postulated to consist of polymer relaxation followed by condensation and pore collapse.

## 1. Introduction

Nogami and Moriya [1], Yamane et al. [2], and Brinker and Mukherjee [3] have recently reported on the direct conversion of monolithic silica [1,2] and borosilicate gels [3] to glasses at temperatures near or below the glass transition temperatures of their conventionally melted counterparts. These reports indicate that the gel-to-glass conversion is dependent on the physicochemical properties of the dried gel and is, therefore, largely determined by the gelation process itself.

The gels described in these previous reports were prepared by the acid or base catalyzed hydrolysis of tetraethylorthosilicate [$Si(OCH_2CH_3)_4$] in alcohol solution to form silanols which subsequently condense to form higher polysilicates. Although hydrolysis and condensation occur concurrently, it is possible to vary the relative rate and extent of each to produce gels which differ markedly in structure and behaviour on heating. The purpose of this work is to relate the nature of the gelation process to the properties of the dried gel and to the gel-to-glass conversion.

* This work was supported by the US Department of Energy (DOE) under Contract DE-AC04-76-DP00789.

** AUS DOE facility.

0022-3093/82/0000–0000/$02.75 

## 2. Experimental

### 2.1. Sample preparation

In order to eliminate effects of phase separation and precipitation, a two-step hydrolysis process was used to prepare all the solutions. The first step consisted of mixing at 60°C tetraethylorthosilicate (TEOS), alcohol (ethanol, n-propanol, or isopropanol), water, and acid (HCl) in a molar ratio 1 : 3 : 1 : 0.0007. This initial water addition equaled one fourth the stoichiometric amount required to fully hydrolyze the TEOS to monosilicic acid. After 1.5 h, additional water plus base ($NH_4OH$) or acid were added for the second hydrolysis step. The investigated compositions lie on a line of equal alcohol/TEOS ratios and vary in water content. These compositions, along with those studied by Aelion et al. [4] and Bechtold et al. [5], are shown in fig. 1 (which for simplicity neglects the pH of the solution). The specific compositions investigated are listed in table 1.

The solutions were maintained at 40°C until gelled. After gelation, the samples were dried slowly at 40°C to produce, in most cases, monolithic specimens which could be machined to specific shapes.

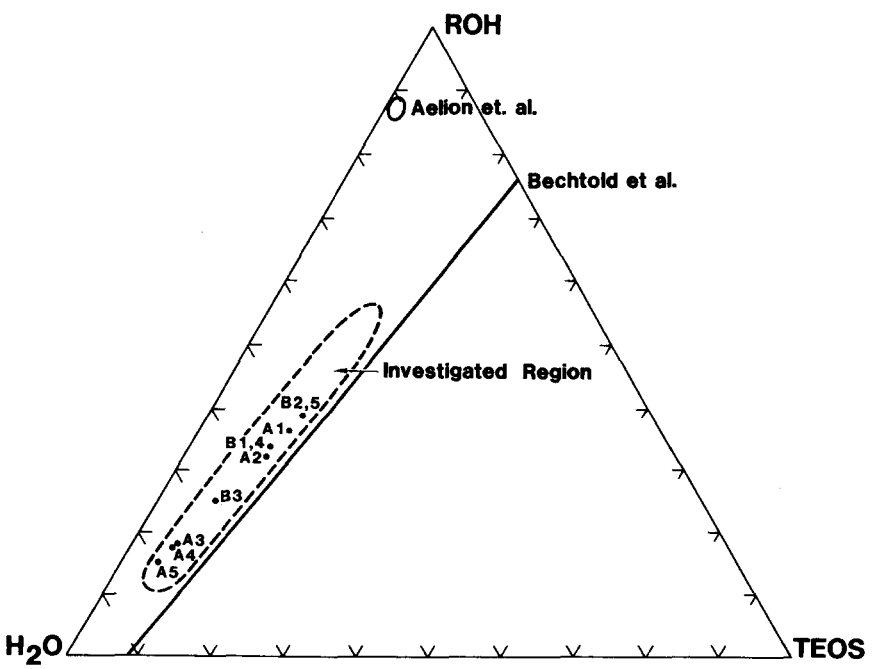


Fig. 1. Compositional region investigated (mol%) along with the region studied by Aelion et al. [4] and the line of compositions studied by Bechtold et al. [5].

Table 1
Compositions investigated (mol%)

| Sample | n-prop | $H_2O$ | TEOS | HCl | $NH_4OH$ | $H_2O$/TEOS |
|---|---|---|---|---|---|---|
| A1 | 36.9 | 50.9 | 12.2 | 0.009 | – | 4.2 |
| A2 | 32.8 | 55.7 | 10.9 | 0.632 | – | 5.1 |
| A3 | 18.4 | 75.5 | 6.1 | 0.005 | – | 12.4 |
| A4 | 17.8 | 76.2 | 6.0 | 0.038 | – | 12.7 |
| A5 | 15.3 | 79.3 | 5.2 | 0.299 | – | 15.3 |
| B2 | 39.2 | 47.9 | 12.9 | 0.010 | 0.016 | 3.7 |
| B3 | 24.7 | 67.0 | 8.3 | 0.006 | 0.027 | 8.1 |
| B5 | 39.4 | 47.1 | 13.0 | 0.010 | 0.611 | 3.6 |

### 2.2. Small angle X-ray scattering (SAXS)

The small angle X-ray data were obtained using the 10 M SAXS system at the National Center for Small Angle Scattering Studies associated with the Oak Ridge National Laboratory. All data were taken at the highest resolution (5 m sample to detector distance) using an X-ray source power of about 2 kW. Run times of 2 to 10 min provided adequate signal to noise ratios. The incident beam wavelength was 1.54 Å characteristic of $CuK_\alpha$ radiation. Samples were supported in a thermostated block maintained to $\pm 1°C$. Samples were thoroughly mixed externally and then inserted into the SAXS sample cells. Sample cells were stainless steel with 0.025 mm thick Mylar windows and a 1 mm path length. The sample transmission coefficient was about 0.3.

### 2.3. Gel characterization

The bulk density, specific surface area and hydrogen and carbon contents of the dried gels were measured as reported previously [3]. Physical and chemical changes which occurred during the gel-to-glass conversion were measured by thermal gravimetric analyses (TGA), differential thermal analyses (DTA), and dilatometry at heating rates of 0.5 to 10°C $min^{-1}$. Densities were calculated from the weight loss and shrinkage. The coarse and fine microstructures of the dried gels were investigated by scanning electron microscopy (SEM) of fractured surfaces and by direct transmission electron microscopy (TEM) of gel fragments, respectively.

## 3. Results and discussion

### 3.1. Small angle scattering results

Small angle X-ray scattering was used to assess structural changes during the gelation process for compositions A1, A2 and B2. The goal of this work

was to characterize the size and growth kinetics of macromolecular clusters. In addition, it was possible to obtain statistical information on the local structure in the case of the base catalyzed gel B2. Typical scattering curves are shown in figs. 2a and 3a. In these figures, $S(K)$ is the scattered intensity as a function of the magnitude of the scattering vector $K$, where $K$ is related to the scattering angle, $\theta$, by:

$$K = (4\pi/\lambda)\sin(\theta/2). \tag{1}$$

The low angle part of the scattering curves (where $K \ll R_g^{-1}$, the so-called Guinier region) was analyzed to yield the mean radius of gyration, $R_g$, of the scattering centers. Distinct differences between the gelation of acid and base catalyzed systems were noted through analysis of the low angle portion of the scattering curves.

The low angle part of the scattering curves of the acid catalyzed gels did not change during the course of gelation, indicating that the size and shape of the silicate molecules (clusters) did not vary. Guinier plots, $\log(I)$ versus $K^2$, (for example fig. 2b) of this part of the scattering curve for A1 and A2 have extended linear regions corresponding to a radius of gyration of 15–17 Å. When the system is dilute, such linearity is indicative of a fairly narrow size distribution of relatively equidimensional molecules.

In contrast, the scattering curve of the base catalyzed gel, B2, changed substantially during the course of the second hydrolysis and subsequent

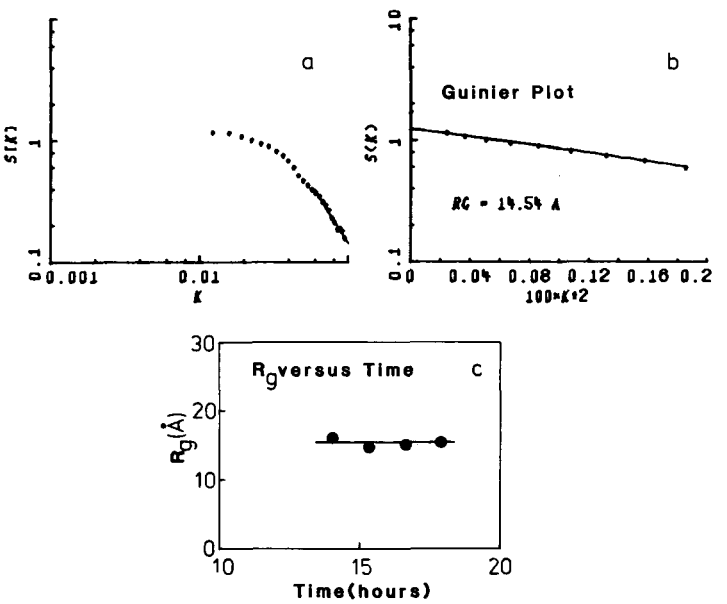


Fig. 2. (a) Typical scattering curve for A2, (b) corresponding Guinier plot, and (c) radius of gyration versus time.

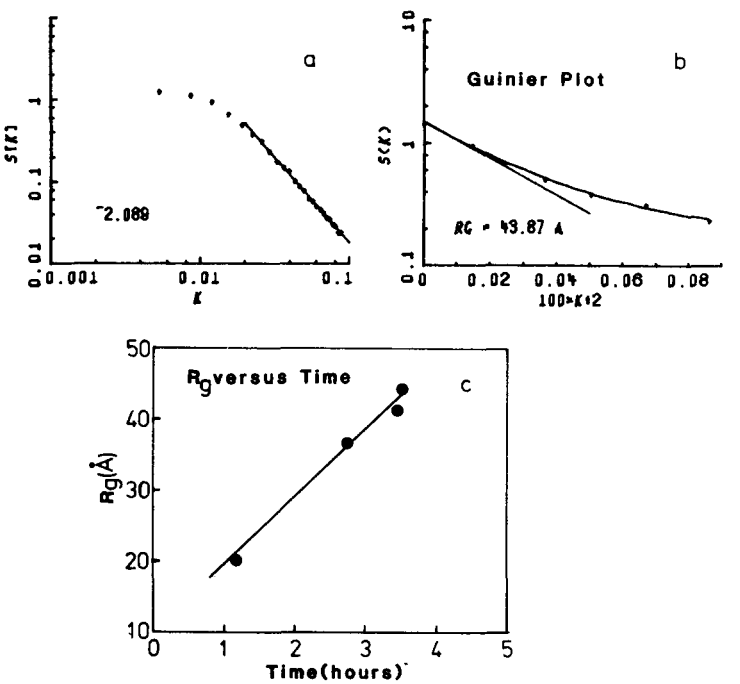


Fig. 3. (a) Typical scattering curve for B2 giving slope of intermediate region, (b) corresponding Guinier plot, and (c) radius of gyration versus time.

gelation. The apparent radius of gyration of the largest molecules grew from 20 Å, 1.2 h after the addition of the base, to 44 Å after 3.8 h, during which time gelation occurred (fig. 3c). The Guinier plots showed marked concavity in these systems throughout the gelation process. In the early more dilute systems where the clusters are independent, this concavity implies polydispersity. After gelation, however, the origin of the concavity is not apparent but may be due either to polydispersity, phase separation, or interchain correlations.

Analysis of the intermediate region of the scattering curve yields information on the detailed structure within a macromolecule. The intermediate region is bounded by the limits $KR_g \gg 1$, $Ka \ll 1$ where $a$ is the size of the silica monomer ($\sim 3$ Å). In the intermediate region, universal power law behavior is predicted which is independent of both the size of the molecule ($R_g$) and the size of the molecular building block ($a$) [6]. In the case of a two-phase system with distinct boundaries for example, the scattering curve $S(K)$ was shown by Porod to vary as $K^{-4}$ [7]. For a random walk polymer chain, by contrast, $S(K)$ should vary as $S(K) \sim K^{-2}$ [8]. Of particular interest to the gelation problem is the prediction of random bond percolation theory which suggests $S(K) \sim K^{-2.6}$.

Unfortunately, power law analysis was not possible in the case of the acid catalyzed gel shown in fig. 2a. Because of the small radius of gyration, the intermediate region ($KR_g \gg 1 \gg Ka$) does not exist.

In the base catalyzed system, power law analysis in the intermediate region shows $S(K) \sim K^{-2}$ (fig. 3a). This result shows that the scattering arises from polymeric structures and not from particles with a definable surface. Unfortunately, the experimental errors in these data do not permit the distinction between a lightly cross-linked, random walk type polymer and the more highly cross-linked type formed by random bond percolation.

### 3.2. Gelation

The small angle scattering results show that the nature of the polymer species is considerably different in acid and base catalyzed gels. This difference can be explained by differences in the relative rates of: (1) hydrolysis of the alkoxide groups to form silanols; (2) condensation of the silanols to form silicate polymers; and (3) linking of the polymers to form a gel. The relative rates of these reactions depend on three factors – the concentrations of water and TEOS and the solution pH. The way in which these relative reaction rates influence the gelation process can best be understood by considering two extreme cases – the case in which hydrolysis proceeds much more rapidly than condensation and the case in which the reverse is true.

In the case of the hydrolysis reaction proceeding much more rapidly than the condensation reaction, there will be only hydroxyl groups and no alkoxy groups bonded to silicon when condensation commences. The most commonly proposed mechanism for the condensation reaction under these conditions is a base-catalyzed, nucleophilic attack on silicon [9];

$$(RO)_3SiOH + OH^- \rightarrow (RO)_3SiO^- + H_2O \qquad \text{(fast)} \tag{2}$$

$$(RO)_3SiO^- + (RO)_3SiOH \rightarrow (RO)_3SiOSi(OR)_3 + OH^-$$

$$\text{(rate determining)}, \tag{3}$$

where $R = H$ or $(RO)_3Si$. The extent of reaction (2) increases with the acidity of the silanol proton on $(RO)_3SiOH$. The acidity of that proton increases as the basicity of the other groups bonded to the silicon decreases, as an example, because $(HO)_3SiO^-$ is a weaker base than $OH^-$, the reaction of monosilicic acid to form the dimer, $(HO)_3SiOSi(OH)_3$, results in an increase in acidity of the silanol groups remaining on the dimer. In general, reaction (2) will occur to a greater extent for a polymer in which the Si is already cross-linked via a bridging oxygen to other Si than for monocilicic acid. Moreover, the more extensive the cross-linking in $(RO)_3SiOH$, the more the acidity of the remaining silanol groups increases. Thus, in a solution of polymers of various degrees of cross-linking, the more cross-linked species will be the most likely to undergo reaction (2) and be available for reaction (3). Conversely, the species least likely to undergo reaction (2) and, hence, the species most likely to participate in reaction (3) in the form $(RO)_3SiOH$ will be the most basic – therefore, least crosslinked – species.

For compositions in which hydrolysis is much more rapid than condensation, the net result of reactions (2) and (3) is that the larger, highly condensed polymers tend to react with feebly acidic monomers to form even more highly condensed species, i.e. the larger polymers grow at the expense of the smaller ones. This can result in a sol of relatively large (50–200 Å) polymers which, due to extensive cross linking, are essentially pure $SiO_2$.

The other extreme case is that of the rate of condensation of silanols (either by dehydration or dealcoholation) being much greater than their rate of production by hydrolysis. This occurs during acid catalyzed hydrolysis at low water and acid concentrations. In this case, the form of the polymers is governed by the mechanisms of the hydrolysis reaction and not by that of the condensation reaction. The acid catalyzed hydrolysis proceeds by a mechanism which involves electrophilic attack on an alkoxide oxygen [4] and, thus, is not particularly sensitive to the electronic effects of the other groups bonded to silicon but would be sensitive to steric effects. Accordingly, monomers are more rapidly hydrolyzed than end groups of chains, which, in turn, are more rapidly hydrolyzed than the middle groups of chains [10]. The silanols on these weakly cross-linked units then condense more rapidly than silanols on more highly cross-linked species are formed, and the resulting polymer is relatively small and not highly cross-linked.

The conditions under which the first stage of hydrolysis is conducted in these experiments are quite similar to this second extreme case (in which hydrolysis is slow with respect to condensation). Therefore, it is expected that after this first hydrolysis, the solution is comprised of small, weakly cross-linked polymers.

Under conditions used for the three different types of second hydrolysis steps, the relative reaction rates are intermediate to the two extreme cases, although in each type the reactions tend more to one extreme than the other. Due to the addition of excess water (more than 2 mol per mol of TEOS) and a base or additional acid catalyst, the rate of hydrolysis is increased with respect to condensation, the amount of this increase being dependent on the particular conditions used. Therefore, the polymers have a tendency both to grow and to condense internally. However, the rate of internal condensation stops when the polymers have weakly cross-linked together to form a rigid gel structure and cannot proceed further until solvent is removed during drying, so that nature of the polymer depends on how rapidly growth and condensation occurs with respect to gelation.

The second hydrolysis of solution A1 and A2 was performed with a relatively low water concentration, so hydrolysis was not greatly accelerated with respect to condensation. The small angle scattering results indicate that almost no change occurs in the size or structure of the polymers, so it appears that they are more likely to weakly cross-link with each other to form a gel than to grow or condense internally. This process produces a gel which is weakly cross-linked compared with the base catalyzed systems described below. The gel remains transparent through the gel point indicating uniformity

and lack of phase separation. The single phase nature of these gels is consistent with the fine texture observed on drying.

Much more water is used in the second hydrolysis of A3, A4 and A5, resulting in a substantial increase in the rate of hydrolysis. This produces many more silanol groups within a given polymer, which permits a greater rate of internal condensation. Also, when two polymers encounter each other, they may condense more extensively with each other to form what is effectively a larger polymer before they cross link with other polymers to form a gel structure. Furthermore, the rate of gelation is slowed by the effective dilution of the solution by the large excess of water. Thus, internal condensation and polymer growth in A3, A4 and A5 can progress further before the onset of gelation than it can in A1 and A2. The resulting gels are slightly translucent and are more particulate in nature.

In the gel series B2, B3 and B5 in which the second hydrolysis is conducted under alkaline conditions, particle growth and internal condensation proceed even faster than in the A3, A4 and A5 series despite the fact that the solutions contain less water. This is due to a number of contributing effects. First, under comparable conditions, the base catalyzed hydrolysis proceeds much faster than the acid catalyzed reaction [4]. Second, the base catalyzed reaction mechanism is a nucleophilic attack by $OH^-$ on Si and, thus, the reactivity toward hydrolysis follows the same pattern as that of condensation, so that the sites that hydrolyze most rapidly will lead to the most condensed product. Third, silica is much more soluble in alkaline solutions than in acidic ones, and the original weakly cross-linked polymers from the first hydrolysis tend to dissolve and reprecipitate on more highly condensed sites.

These processes would produce the cluster growth observed in the small angle scattering experiments. It should also be pointed out that the coarse texture of the base catalyzed systems may be due to phase separation into solvent-rich and polymer-rich regions. Both experimental and theoretical evidence suggests that phase separation will occur as cross-linking proceeds. Topologic and kinetic limitations prohibit macroscopic phase separation and lead to separation on a microscopic scale resulting in a translucent system.

### *3.3. Dried gel microstructures*

The physical differences between gels of rapidly and slowly hydrolyzed solutions are clearly illustrated by comparisons of the respective microstructures of the dried gels as shown in figs. 4 and 5.

Gels A1 and A2, prepared under conditions of slow hydrolysis, exhibit extremely fine microstructural features ($\sim 50$ Å) and do not appear to be particulate. This is consistent with the SAXS results and the mechanisms of gelation. The low electron density contrast seen in the TEM micrographs suggests that for samples A1 and A2 the pores must be much finer and more evenly distributed throughout the gel. This results in a dry gel which is optically clear and relatively dense. In contrast, gels A3–A5 and B2–B5 show

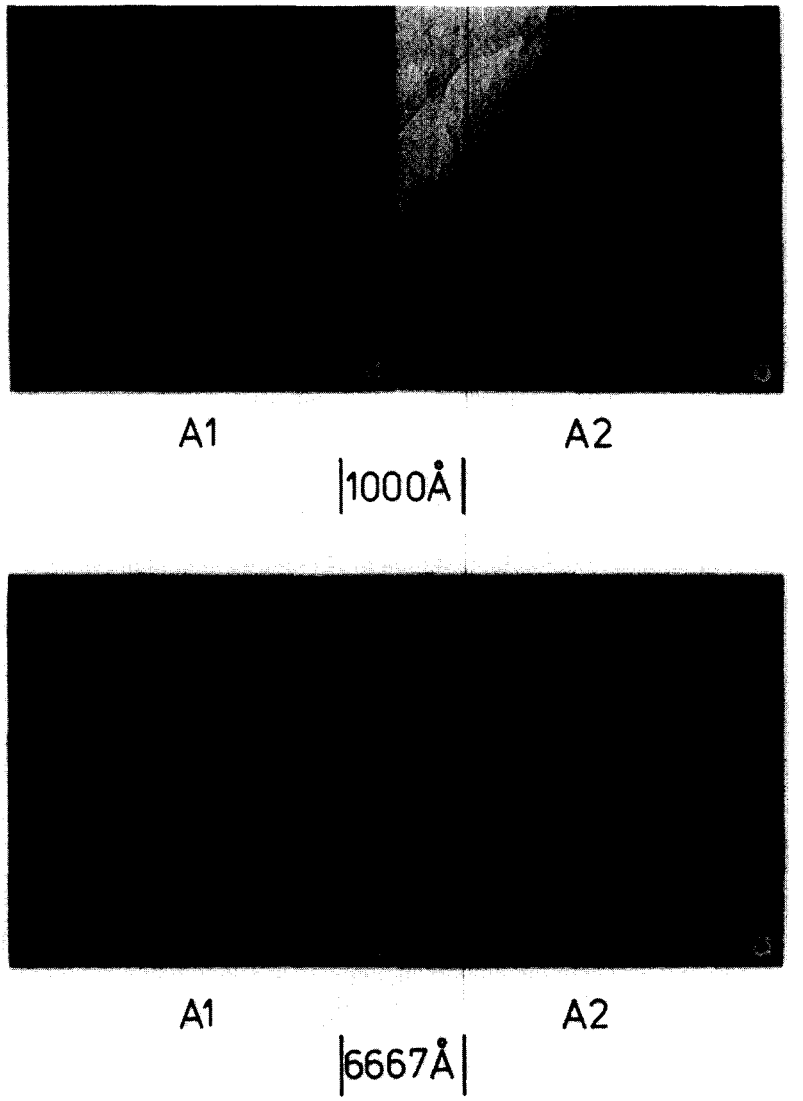


Fig. 4. (a) Direct TEM micrograph of A1, (b) direct TEM micrograph of A2, (c) SEM micrograph of A1, and (d) SEM micrograph of A2.

larger microstructural features and appear to be particulate on two different dimensional scales. For example, B2, prepared at the highest pH (of gels shown in figs. 4 and 5), appears to consist of coarse ($\sim 900$ Å) particles which in turn are made up of much smaller ($\leq 100$ Å) particles. The high (electron density) contrast seen in the TEM micrograph of B2 requires there exist fairly large dense regions which are surrounded by equally large regions of quite low

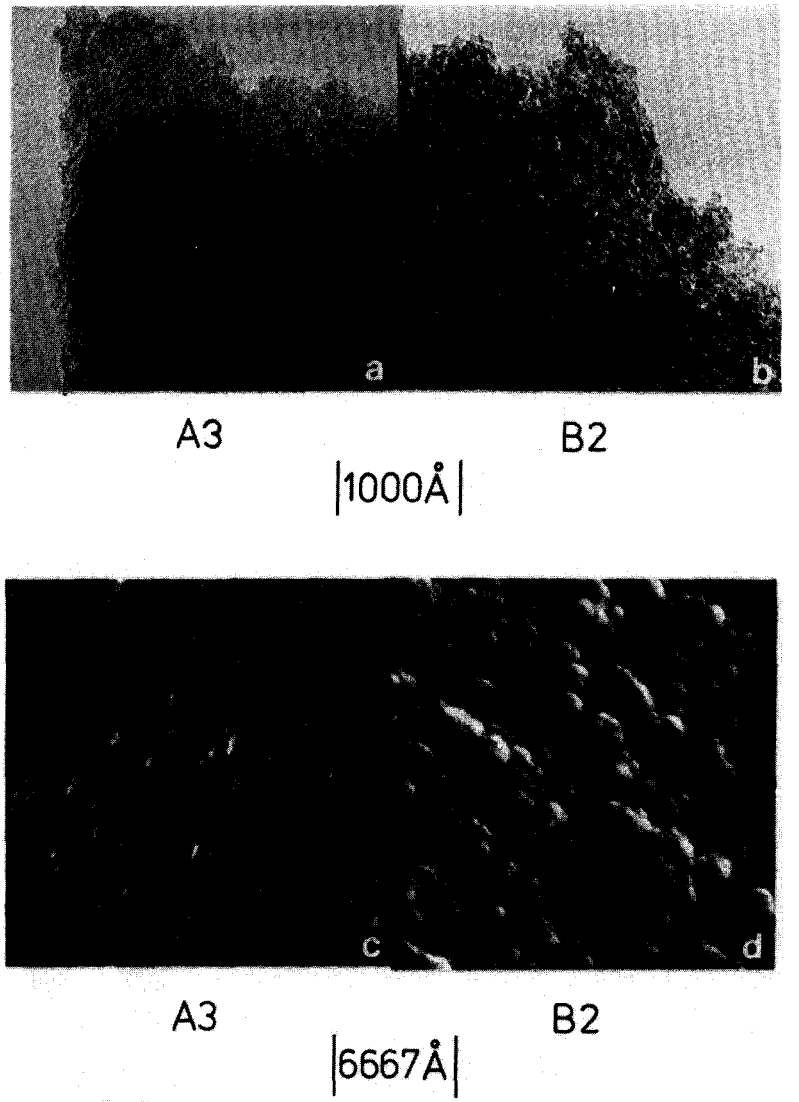


Fig. 5. (a) Direct TEM micrograph of A3, (b) direct TEM micrograph of B2, (c) SEM micrograph of A3, and (d) SEM micrograph of B2.

density. This results in a translucent gel of low bulk density. The large particles observed in fig. 5d are not well bonded together, so that slight abrasion results in the formation of a fluffy powder. Gel A3, prepared with a high water concentration and at an intermediate pH (conditions under which hydrolysis is expected to be fast compared with A1 but slow compared with B2), exhibits

many of the features of B2 but on a finer scale. The resultant dried gel is slightly translucent and hard compared with B2.

Electron microscope observations indicate that the different structures of the slowly and rapidly hydrolyzed gels respond differently to the removal of solvent during drying. Upon removal of solvent, both the individual polymer units comprising the gel and the gel structure itself may shrink. This permits additional condensation reactions within and between polymers. In the slowly hydrolyzed, acid catalyzed gels prepared with low water contents (A1 and A2), strong surface tension forces are generated by removal of solvent from the small solvent-rich regions between the polymers. As the weakly cross-linked polymers impinge on one another, they deform readily and form a dense gel structure. At the same time as solvent is removed from within the solution shell of the polymer, the polymer itself can readily shrink and form more cross links. The overall result is a very dense dried gel with no large voids and no identifiable polymers. When the hydrolysis is more rapid (e.g. B2), the polymers are larger and more highly cross-linked; therefore, upon impingement, the polymers will not deform as readily to fill the voids nor will they shrink as much due to removal of solvent from within the polymer. The gel then dries to a more or less random packed array of identifiable particles around which are large voids.

The observed gel microstructures agree with both the SAXS results and the concepts of gelation. That is, gels prepared under conditions where hydrolysis is slow exhibit extremely fine features and dry to a high bulk density while gels prepared under conditions where hydrolysis is fast are particulate and dry to a low bulk density.

### *3.4. Physical properties of dried gels*

The results of the physical and chemical property measurements are summarized in tables 2 and 3. Carbon and hydrogen contents measured by combustion analysis were converted to EtO/Si and OH/Si by assuming that carbon was present only as ethoxyde (that is by assuming no adsorbed solvent and no transesterification) and that all adsorbed water was removed before the analysis. The number of bridging oxygens per silicon (O/Si) was calculated by assuming: $\mathrm{EtO/Si} + \mathrm{OH/Si} + 2(\mathrm{O/Si}) = 4$.

Within the acid catalyzed series, higher water concentrations resulted in greater extents of hydrolysis (decreased EtO/Si ratios) and, with the exception of A3, greater extents of condensation (increased O/Si ratios). However due to their particulate nature, the resultant gels showed a systematic decrease in both bulk density and surface area per unit volume. These changes in physical properties with water content are represented graphically in fig. 6 for acid catalyzed gels.

Acid additions at constant water content also appear to promote both hydrolysis and condensation as evidenced by comparing A4 (0.038 mol% HCl)

Table 2
Summary of physical properties

| Samples | $H_2O/Si$ | Apparent pH | Gel time (h) | Density ($g\,cm^{-3}$) | Surface area ($m^2\,g^{-1}$) | Surface area ($m^2\,cm^{-3}$) |
|---|---|---|---|---|---|---|
| A1 | 4.2 | 2.7 | 77 | 1.63 | 734 | 1196 |
| A2 | 5.1 | 0.8 | 25 | 1.54 | 740 | 1139 |
| A3 | 12.4 | 3.1 | 12 | 1.42 | 806 | 1144 |
| A4 | 12.7 | 2.1 | 27–90 | 1.39 | – | – |
| A5 | 15.3 | 1.4 | 27–90 | 1.32 | – | – |
| B2 | 3.7 | 7.9 | 4 | 0.99 | 910 | 901 |
| B3 | 8.1 | 8.2 | 2 | 0.84 | – | – |
| B5 | 3.6 | 8.8 | 0.2 | 0.68 | – | – |

Table 3
Calculated silicon environment: $EtO/Si + OH/Si + 2(O/Si) = 4$

| Sample | EtO/Si | OH/Si | O/Si |
|---|---|---|---|
| A1 | 0.35 | 0.33 | 1.66 |
| A2 | 0.22 | 0.39 | 1.69 |
| A3 | 0.19 | 0.53 | 1.64 |
| A4 | 0.02 | 0.47 | 1.75 |
| A5 | 0.01 | 0.42 | 1.79 |
| B2 | 0.21 | 0.33 | 1.73 |
| B3 | 0.10 | 0.23 | 1.83 |
| B5 | 0.12 | 0.30 | 1.79 |

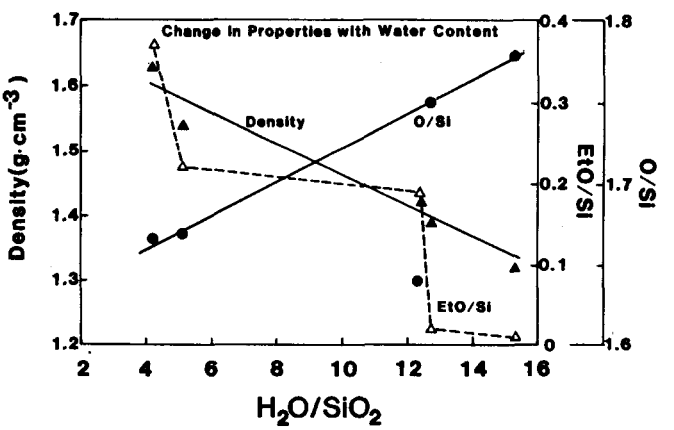


Fig. 6. Density, EtO/Si, and O/Si as a function of water content for acid catalyzed gels.

to A3 (0.005 mol% HCl). The resulting more highly cross-linked gel again showed reduced bulk density.

The most striking feature of base catalyzed gels was their very low bulk densities. Density appeared to be inversely related to catalyst concentration rather than inversely related to water content as was the case for the acid catalyzed series. Comparisons of samples B2 and B5 show that, at a constant water content, $NH_4OH$ additions greatly promote hydrolysis (reduced EtO/Si ratios) but only slightly increase polymerization. Comparison of samples B5 and B2 to A1 show that, at similar water contents, hydrolysis and condensation are much more extensive in the base catalyzed gels, while bulk density and surface area (per unit volume) are greatly reduced.

### *3.5. Gel-to-glass conversion*

During the gel-to-glass conversion, both chemical and structural transformations take place which can be summarized as follows [2,3]: (1) physical desorption of water and solvents from micropore walls; (2) carbonization and combustion of residual organic groups; (3) condensation polymerization; (4) volume relaxation; and (5) viscous sintering. Of these transformations (3), (4) and (5) result in densification; therefore, it is expected that gels of different chemical compositions and morphologies should show markedly different densification behavior.

Gel behavior during the conversion was monitored by DTA, TGA, and shrinkage. The results are shown in figs. 7, 8 and 9.

In fig. 7, the prominent endothermic DTA features are attributed to desorption of physically adsorbed water (100–150°C) and carbonization of residual alkoxy groups (200–300°C). The exothermic combustion of carbon occurs between 275°C and 400°C. Gel A1 (calculated to have the highest EtO/Si ratio) shows the largest combustion exotherm. Likewise, gel A4 (calculated to have a very low EtO/Si ratio) shows no identifiable exotherm. Comparison of A3 with A4 again demonstrates that, for gels prepared with the same water content, acid additions promote hydrolysis (reduced EtO/Si ratios).

Weight loss corresponding to the desorption of water, combustion of carbon, and condensation polymerization is shown in fig. 8. The weight loss due to combustion (275–400°C) scales with the calculated EtO/Si ratio. Weight loss continues to high temperatures presumably due to the continued removal of water by condensation reactions.

Shrinkage measurements (fig. 9) show a large temperature dependence. Within the acid catalyzed series, the temperature corresponding to the onset of rapid shrinkage scales with the cross-link density and varies from about 600°C for A1 and A2 to about 800°C for A5. The base catalyzed gel, B2, shows an increased shrinkage rate at about 900°C.

Shrinkage measurements were combined with weight loss measurements to calculate densification as a function of temperature as shown in fig. 10. Within the temperature range investigated ($\leq 900$°C), only the acid catalyzed gels

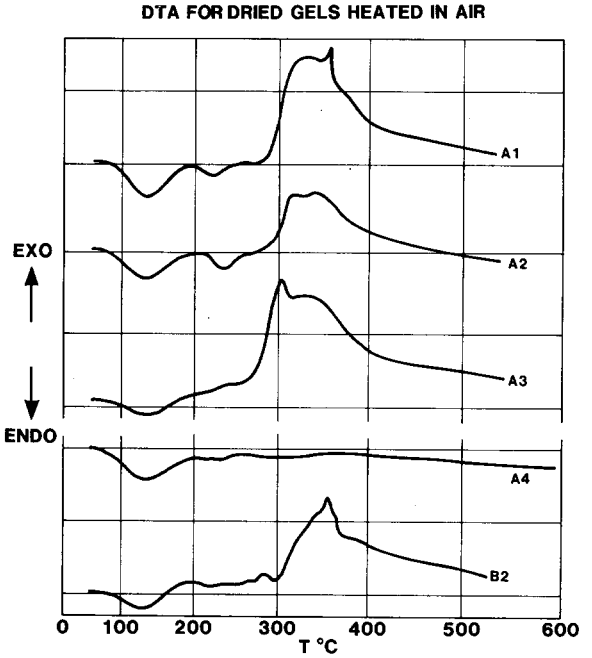


Fig. 7. DTA curves for equal weights of dried gels heated in air at 10°C $min^{-1}$.

approached full density at a heating rate of 1°C/min. Although both A1 and A2 showed increased shrinkage beginning at 600°C, only A2 completely densified. Residual organics and water entrapped within A1 caused bloating and reduced density. All of the base catalyzed gels investigated began to densify significantly at about 900°C. Their behavior is well represented by B2.

Gels A2 and B2 exhibit densification behavior somewhat similar to that reported by Nogami and Moriya [1] for acid and base catalyzed gels prepared

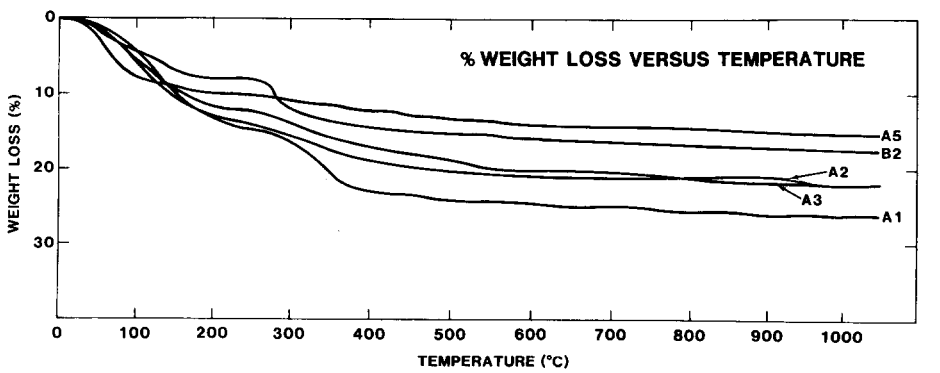


Fig. 8. Weight loss (%) versus heat treatment temperature.

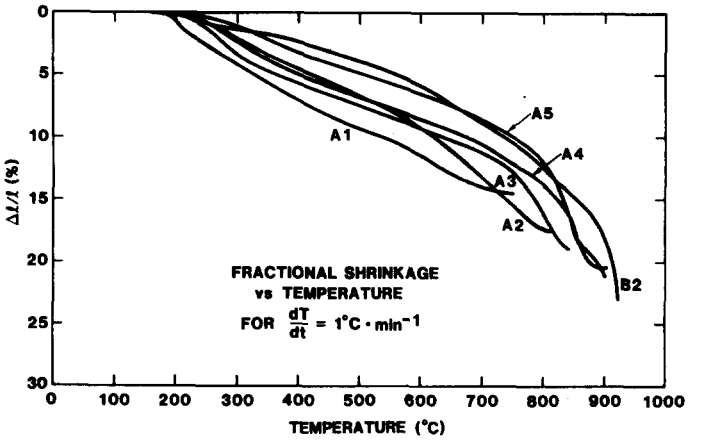


Fig. 9. Fractional linear shrinkage for gels heated in air at 1°C $min^{-1}$.

with 10 mol of water per mol of TEOS. In their report, Nagami and Moriya attributed the high temperature densification of base catalyzed gels to viscous sintering; however, no densification model could be satisfactorily applied to the observed shrinkage of acid catalyzed gels.

To further investigate possible densification mechanisms, fractional shrinkage versus temperature data obtained at a constant heating rate (fig. 9) were replotted as the logarithm of the fractional shrinkage versus $1/T°K$ (fig. 11). Plotted in this manner, a change in slope represents a change in mechanism and/or gel structure [8–10]. The curves obtained for the acid catalyzed gels are roughly parallel below 8.2% linear shrinkage ($\ln \Delta l/l = -2.5$) with the curves shifted to higher temperatures for increased extents of crosslinking for both the

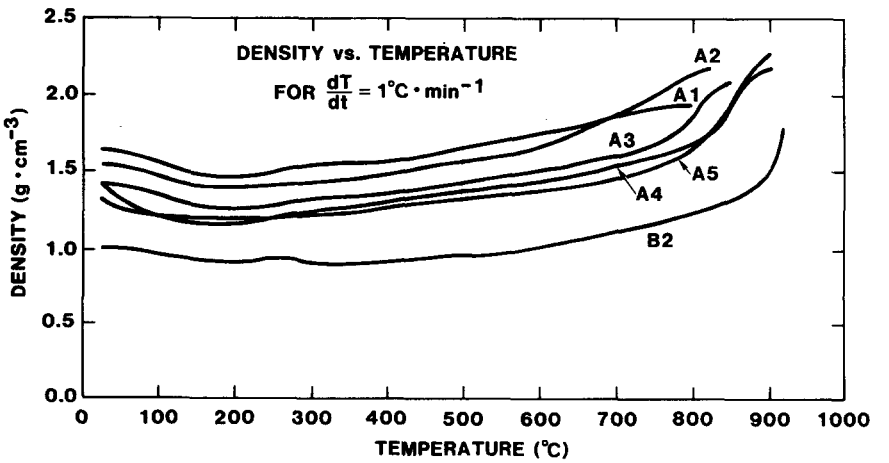


Fig. 10. Calculated density versus heat treatment temperature for gels heated at 1°C $min^{-1}$.

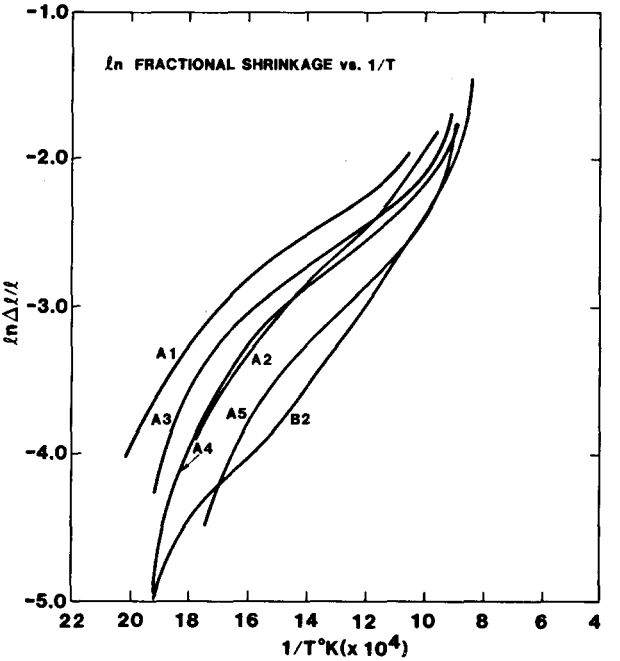


Fig. 11. Natural logarithm of fractional shrinkage versus inverse absolute temperature.

particulate (A3–A5) and the non-particulate (A1 and A2) gels. The curves obtained for base catalyzed gels, represented by curve B2, are shifted to even higher temperatures and at low shrinkage (< 13.5%) do not appear to parallel the curves obtained for acid catalyzed gels. Above 13.5% shrinkage ($\ln \Delta l/l = -2.0$), the slopes of curves A3, A4 and A5 rapidly increase to approach the slope of curve B2 while the slope of curve A2 (A1 was not plotted above 650°C due to bloating) remains significantly lower throughout the complete densification process.

These results indicate a difference in high temperature densification mechanisms between particulate and non-particulate gels and a difference in low temperature densification mechanisms between acid and base catalyzed gels. High temperatures are required to densify particulate gels by viscous sintering. The large values observed for slopes of curves A3–A5 and B2 are attributable to the large activation energy for viscous sintering ($\sim 170$ kcal mol$^{-1}$). In contrast a lower temperature (800°C) was sufficient to density gel A2. The lower value obtained for the slope of curve A2 suggests that final densification occurs by a mechanism other than viscous sintering. These differences in densification mechanisms are for the most part explained by both the amount and distribution of non-condensed O*R* and OH groups in the dried gels.

Gels A1 and A2, which were not observed to be particulate by electron microscopy and which were determined to have small radii of gyration by

SAXS, are less hydrolyzed and less polymerized than A4, A5 or B2. Therefore, gels A1 and A2 contain larger amounts of non-condensed O*R* and OH groups, which due to the observed extremely fine pore size and apparent uniformity of electron density (figs. 5a and 5b), are likely to be more uniformly distributed thoughout the dried gels. If, for example, the 0.68 (EtO + OH) groups per silicon atom are uniformly distributed throughout gel A1, on the average only 3.3 out of 4 oxygens surrounding each silicon are bridging oxygens. The resultant gel structure might then be considered to consist of a sponge-like structure. The porosity would be then limited to very fine channels within the sponge and would create, at the interior of each channel, a negative pressure inversely proportional to the channel radius. At low temperatures, this negative pressure, which is equivalent to an equal positive pressure on the gel exterior, would be the driving force for rearrangements or relaxations of the entangled polymers, and, at higher temperatures, the external pressure would contribute to collapsing of the micropores. Both relaxation processes and micropore collapse combined with additional cross-linking are expected to produce a dense gel at low temperatures.

TEM observations suggest that B2 might consist of highly polymerized silica particles, the surfaces of which would contain more of the non-condensed species. The very low measured bulk densities could then result from the random packing of the observed large ($\sim 900$ Å) spheres which, in turn, consist of a random packing of the observed smaller ($\sim 100$ Å) dense particles. This type of packing would result in a density of approximately $(0.66)^2 \times 2.2 \simeq 0.96$. (Lower densities would arise, if the particles were arranged in chains to form a totally interconnected array with a lower number of particles.) In either case, heating at low temperatures could only be expected to react one dense particle with its neighbor or rearrange the particles into a more densely packed array. High temperatures would be required for complete densification by viscous sintering. Because the average pore size for B2 is much greater than for gels A1–A5, the driving force for sintering would be reduced, thus increasing the sintering temperature.

Gels A3, A4 and A5 appeared to be particulate (e.g. fig. 5a) but on a much finer scale than B2. If, due to the acid catalysis, the particles are less internally polymerized than in base catalyzed gels, it is expected that low temperature densification of individual particles would occur as in A1 or A2. However, because of their particulate nature, high temperatures would be required for complete densification. The finer average pore size of gels A3–A5 compared with B2 should reduce the required sintering temperature.

## 4. Conclusions

Differences in the rates of hydrolysis relative to the rates of condensation during the gelation process resulted in very different polymer structures at the gel point. When hydrolysis was rapid compared with condensation (e.g. B2)

larger, more highly condensed silicate polymers were formed. In the reverse case, when condensation was rapid compared with hydrolysis (e.g. A1 and A2) smaller, less condensed polymers were formed. During drying, these two types of gels were transformed to low density particulate gels and high density non-particulate gels, respectively.

On heating, the particulate gels were converted to dense glasses at high ($>800°C$) temperatures by a viscous sintering process. Differences in the specific temperature required by each gel were related to differences in the microstructures of the dried gels. Higher temperatures were required for gels with coarser microstructures.

The gels which were not observed to be particulate (e.g. A1 and A2) began to densify significantly at 600°C. This low temperature densification was explained by a process consisting of polymer relaxation followed by condensation and pore collapse. This process was possible due to the larger amount of randomly distributed ($OH + OR$) groups existing in the less highly condensed gels and their much finer pore size.

The results of this investigation indicate that the gel-to-glass conversion is highly dependent on the sol-to-gel transition. This implies that optimization of the solution conditions will serve to minimize the gel to glass conversion temperature and, therefore, result in lower temperature applications for sol–gel derived glasses.

The authors would like to thank M.M. Sturm and W.R. Sorenson for the electron microscopy and B.M. Schwartz, N.A. Durand and J.C. Lanoue for contributions to the experimental content of this paper. J.S. Lin and P. Labarbe of the National Center for Small Angle Scattering Studies provided much assistance with the X-ray experiments.

## References

[1] M. Nogami and Y. Moriya, J. Non-Crystalline Solids 37 (1980) 191.
[2] M. Yamane, S. Aso, S. Okano and T. Sakaino, J. Mat. Sci. 14 (1979) 607.
[3] C.J. Brinker and S.P. Mukherjee, J. Mat. Sci. 16 (1981) 1980.
[4] R. Aelion, A. Loebel and F. Eirich, J. Am. Chem. Soc. 72 (1950) 5705.
[5] M.F. Bechtold, R.D. Vest and L. Plambeck, Jr., J. Am. Chem. Soc. 90 (1968).
[6] D.W. Schaefer, J.F. Joany and P. Pincus, Macromol. 13 (1980) 1280.
[7] G. Porod, Kolloid Z. 124 (1951) 83.
[8] P.G. de Gennes, Scaling concepts in polymer physics (Cornell University Press, Ithaca, New York, 1979).
[9] R.K. Iler, The chemistry of silica (John Wiley, New York, 1979).
[10] K.A. Andrianov, Organic silicon compounds (State Scientific Technical Publishing House for Chemical Literature, Moscow, 1955.
[11] W. Young and I. Cutler, J. Am. Ceram. Soc. 53 (1970) 659.
[12] J.L. Woolfrey and M.J. Bannister, J. Am. Ceram. Soc. 55 (1972) 390.
[13] M.J. Bannister, J. Am. Ceram. Soc. 51 (1968) 209.